could bring within reach the production of photonic-bandgap materials[4–6] at optical wavelengths. □

Methods

Stable nonaqueous emulsions were obtained with formamide (98%) as the polar liquid and isooctane (>99%) as the oil. Before emulsification, the oil was mixed with ~1% of silicone oil to prevent Ostwald ripening[16]. The surfactant was a symmetric triblock copolymer, poly(ethylene glycol)–poly(propylene glycol)–poly(ethylene glycol) with a relative molecular mass of 5,800 containing 30% by weight of ethylene glycol monomer (Aldrich). Emulsification was done with a homogenizer. The emulsion was fractionated as described by Bibette[12].

The preparation of the ceramic precursor solution is described with the titania synthesis as an example, because it requires the most reactive alkoxide which is the most difficult to handle. Titanium tetraisopropoxide (97%) was treated with an equimolar amount of the chelating agent 2,4-pentanedione to reduce its reactivity towards water[21]. It was then mixed rapidly by stirring with a mixture of water and formamide, such that the resulting H_2O/Ti molar ratio was 3.5 and the Ti concentration was 2.0 M. The resulting clear yellow solution contains a considerable amount of isopropanol produced by the hydrolysis reaction. Because alcohol will destabilize the emulsion, it was removed by double extraction with a fivefold excess of hexanes. The resulting yellow liquid was often turbid. The sol was heated briefly to ~90 °C producing a clear yellow, slightly viscous sol, which did not form a precipitate for several weeks. Zirconia sols were prepared in an analogous fashion, starting with zirconium tetra-*n*-butoxide (70% in *n*-butanol). Silica sols were prepared by vigorously mixing silicon tetramethoxide with a mixture of water and formamide acidified to pH 2 with HCl.

The surfactant was dissolved to 2 wt% in the sol. For nonuniform pore materials the oil was emulsified directly into it. For uniform pores the separately prepared monodisperse emulsion was centrifuged and the cream dispersed in the sol. The droplet volume fraction was then set by centrifugation and removal of the clear yellow fluid at the bottom. Then 30% ammonia was added so that the molar ratio NH_3/Ti ≈ 1. The increase in pH induces gelation in about 3 h. Gels were aged at 50 °C for 24 h in closed 2-ml polyethylene vials, then allowed to exchange pore fluids with excess ethanol for 24 h. The gels were then dried at room temperature and calcined in air in a furnace.

Received 27 February; accepted 11 August 1997.

1. Yablonovitch, E. Photonic band-gap structures. *J. Opt. Soc. Am. B* **10,** 283–295 (1993).
2. Joannopoulos, J. D., Meade, R. D. & Winn, J. N. *Photonic Crystals: Molding the Flow of Light* (Princeton Univ. Press, 1995).
3. Soukoulis, C. *Photonic Band Gap Materials* (Kluwer, Dordrecht, 1996).
4. Flaugh, P. L., O'Donnel, S. E. & Asher, S. A. Development of a new optical wavelength rejection filter: Demonstration of its utility in Raman spectroscopy. *Appl. Spectrosc.* **38,** 847–850 (1984).
5. Harold, M. P. *et al.* Catalysis with inorganic membranes. *MRS Bull.* **19,** 34–39 (1994).
6. Bhave, R. R. *Inorganic membranes synthesis, characteristics, and applications* (Van Nostrand Reinhold, New York, 1991).
7. Wu, M. X., Fujiu, T. & Messing, G. L. Synthesis of cellular inorganic materials by foaming sol gels. *J. Non-Cryst. Solids* **121,** 407–412 (1990).
8. Litovsky, E., Shapiro, M. & Shavit, A. Gas pressure and temperature dependences of thermal conductivity of porous ceramic materials. 2. Refractories and ceramics with porosity exceeding 30%. *J. Am. Ceram. Soc.* **79,** 1366–1376 (1996).
9. Singer, P. Low k dielectrics: the search continues. *Semicond. Int.* **19,** 88–96 (1996).
10. Beck, J. S. *et al.* A new family of mesoporous molecular sieves prepared with liquid crystal templates. *J. Am. Chem. Soc.* **114,** 10834–10843 (1992).
11. Krauss, T., Song, Y. P., Thoms, S., Wilkinson, C. D. W. & DelaRue, R. M. Fabrication of 2-D photonic bandgap stuctures in GaAs/AlGaAs. *Electron. Lett.* **30,** 1444–1446 (1994).
12. Bibette, J. Depletion interactions and fractionated crystallization for polydisperse emulsion purification. *J. Colloid. Interface Sci.* **147,** 474–478 (1991).
13. Brinker, C. J. & Scherer, G. W. *Sol-Gel Science* (Academic, San Diego, 1990).
14. Pusey, P. N. & van Megen, W. Phase behaviour of concentrated suspensions of hard colloidal spheres. *Nature* **320,** 340–342 (1986).
15. Walsh, D. & Mann, S. Fabrication of hollow porous shells of calcium carbonate from self-organizing media. *Nature* **377,** 320–323 (1995).
16. Imhof, A. & Pine, D. J. Stability of nonaqueous emulsions. *J. Colloid Interface Sci.* (in the press).
17. Dinsmore, A. D., Yodh, A. G. & Pine, D. J. Entropic control of particle motion using passive surface microstructures. *Nature* **383,** 239–242 (1996).
18. van Blaaderen, A., Ruel, R. & Wiltzius, P. Template-directed colloidal crystallization. *Nature* **385,** 321–324 (1997).
19. Hachisu, S. & Yoshimura, S. Optical demonstration of crystalline superstructures in binary mixtures of latex globules. *Nature* **283,** 188–189 (1980).
20. Bartlett, P., Ottewill, R. H. & Pusey, P. N. Superlattice formation in binary mixtures of hard-sphere colloids. *Phys. Rev. Lett.* **68,** 3801–3804 (1992).
21. Sanchez, C., Babonneau, F., Doeuff, S. & Leaustic, A. in *Ultrastructure Processing of Advanced Ceramics* (eds Mackenzie, J. D. & Ulrich, D. R.) 77–87 (Wiley, New York, 1988).

Acknowledgements. We thank F. Lange and G. Stucky for discussions, and Q. Huo for help with the adsorption measurements.

Correspondence should be addressed to D.J.P. (e-mail: pine@engineering.ucsb.edu).

Experimental determination of the organic carbon flux from open-ocean surface waters

S. Emerson*, P. Quay*, D. Karl†, C. Winn†, L. Tupas† & M. Landry†

* *School of Oceanography, University of Washington, Seattle, Washington 98195, USA*

† *Department of Oceanography, University of Hawaii, Honolulu, Hawaii 96822, USA*

The flux of biologically produced organic carbon from the euphotic zone of the ocean to the deep waters below—the 'biological organic carbon pump'—is one of the main controls on the carbon dioxide partial pressure in the atmosphere[1]. Accurate determination of this flux is therefore critically important for understanding the global carbon cycle and its response to climate change. Our goal is to assess how accurately the biological organic carbon pump can be determined at a single location and to constrain estimates of the global value. As there are no standards against which such environmental fluxes can be measured, we assess accuracy by comparing results from three independent experimental approaches for measuring the net annual export of organic carbon from the euphotic zone in the subtropical North Pacific Ocean near Hawaii. Mass balances of dissolved oxygen, inorganic carbon and organic carbon yield estimates of the organic carbon export flux of 2.7 ± 1.7, 1.6 ± 0.9 and 2.0 ± 0.9 mol C m^{-2} yr^{-1}, respectively. These three estimates are not significantly different, and establish the present analytically attainable accuracy at this location to be about ±50%. If 2.0 mol C m^{-2} yr^{-1} is typical of the organic carbon export flux in the subtropical ocean, then this vast region, often considered to be a biological desert, may be responsible for up to half of the global-ocean biological organic carbon pump.

The United States JGOFS (Joint Global Ocean Flux Study) Pacific time-series station[2] (station ALOHA of the Hawaii Ocean Time series) is located in the southeastern region of the anticyclonic subtropical gyre at 22° 45′ N, 150° W. Particulate carbon fluxes have been determined over the duration of the programme using drifting sediment traps[3], as have measurements of the dissolved inorganic carbon (DIC) concentration[4] and its stable-isotope ratio[5] ($^{13}C/^{12}C$). Monthly measurements of the concentrations of the gases O_2, N_2 and Ar were made during the years 1990[6], 1992 and 1995.

The biological consumption of DIC (J_{DIC} in mol C m^{-2} yr^{-1}) in the euphotic zone of the ocean is equal to the net production of particulate inorganic carbon (PIC) as $CaCO_3$ (J_{PIC}) and organic carbon (J_{OC}) in both dissolved and particulate forms (J_{DOC} and J_{POC}, respectively):

$$J_{DIC} = J_{PIC} + J_{OC} = J_{PIC} + J_{DOC} + J_{POC} \quad (1)$$

Sediment trap collections and alkalinity/DIC ratios in the upper thermocline[7] at station ALOHA indicate that the flux of PIC out of the upper ocean is only about one-tenth of the total particulate carbon flux; thus, we focus on the net biological production rate of organic carbon, which is stoichiometrically related to the net production of oxygen (J_{O_2}) via the production quotient[8], β:

$$J_{OC} = \beta J_{O_2} \quad (2)$$

Our approach is to evaluate each of the production terms in these equations by determining mass balances of DIC, oxygen and organic carbon.

Nature © Macmillan Publishers Ltd 1997

The mass balance of dissolved species, A, in the upper ocean at this location can be expressed as:

$$h[\mathrm{d}(\bar{A}/\mathrm{d}t)] = F_{a-w} + F_h - V\Delta\bar{A} \pm J_A \quad (3)$$

The over-bar indicates the mean value over the upper 100 m, which approximates the depth of the winter mixed layer, h, and the transition from net community O_2 production to net community respiration[6]; F_{a-w} is the gas exchange flux, and F_h is the flux between the mixed layer and the top of the thermocline. The latter value includes the Ekman downwelling and all other 'vertical' transport processes. Surface horizontal advection is modelled as a flow rate, V (in cm s^{-1}), multiplied by the difference in dissolved concentration between the upstream and local concentrations, $\Delta\bar{A}$. The net biological production or consumption term is indicated by J_A.

Net biological oxygen production is determined from dissolved O_2, N_2 and Ar concentrations measured at roughly monthly intervals for the years 1990, 1992 and 1995 (Fig. 1). The positive difference between the degree of oxygen and argon supersaturation (Fig. 1a) is a qualitative measure of the biological oxygen production[6] in the euphotic zone. The gases are supersaturated in surface waters during the entire year (Fig. 1b), indicating a net diffusive transport to the atmosphere. Air–water exchange rates, F_{a-w}, are modelled as the sum of a bubble flux term, B, and a diffusion term[9–11] which is the product of a mass transfer coefficient, G (in m d^{-1}), and the degree of gas saturation:

$$F_{a-w} = B + G\{S(p_C) - [C]\} \quad (4)$$

where p_C is the partial pressure of gas C (in atm) in the atmosphere, S is the gas solubility (in mol m^{-3} atm^{-1}), and [C] is the gas concentration (in mol m^{-3}) in the mixed layer. For relatively insoluble gases, the bubble term is influential in causing gas supersaturation (see Fig. 1 legend). The mass transfer coefficient is evaluated from daily averaged wind speed measurements on a nearby buoy[6] and correlations to wind speed[12,13] (mean annual value, 2.7 m d^{-1}). Horizontal velocities, V, are determined to be 1–2 cm s^{-1} from the northward component of climatological ship drift speeds and geostrophic calculations[14]. With these independent transport estimates, three simultaneous equations for N_2, Ar and O_2 are used to calculate O_2 fluxes via bubble transport, B, vertical exchange between the surface ocean and thermocline, F_h, and the net biological oxygen production rate, J_{O_2}. The mass balance described in equation (3) is solved using a three-layer, two-dimensional model that separates the mixed layer, the mixed layer to 100 m depth, and the upper thermocline (see ref. 6 for details of the model.)

The oxygen mass balance indicates that net biological O_2 production in the euphotic zone is roughly balanced by losses to the atmosphere and the thermocline. The annual rate of change of O_2 concentration and the horizontal flow of O_2 are less than one-tenth the value of the other terms. Oxygen loss to the atmosphere averages -1.6 mol O_2 m^{-2} yr^{-1} for the 3 years. This is the net gas exchange value which consists of the difference between outgassing driven by the surface ocean supersaturation (Fig. 1b) at a rate of -2.6 mol m^{-2} yr^{-1} and the bubble-induced invasion rate of 1.0 mol m^{-2} yr^{-1}. Downward transport to the top of the thermocline is -1.5 mol m^{-2} yr^{-1} which probably results from turbulent mixing or eddy-induced dipycnal transport[15], as Ekman velocities[14] can account for only a small fraction of this flux. Oxygen losses from the upper ocean are balanced by a net biological oxygen production of 3.6 ± 2.2 mol m^{-2} yr^{-1}, which is equivalent to an organic carbon production rate of 2.7 ± 1.7 mol C m^{-2} yr^{-1}. The conversion from oxygen fluxes to carbon fluxes and error estimates are described in Table 1.

Dissolved inorganic carbon and carbon isotope ($DI^{13}C$) measurements at station ALOHA are used to determine the net biological carbon export[5,6]. We derive independent information from these two budgets because $DI^{13}C$ has an equilibration time with the atmosphere via gas exchange that is approximately ten times that of DIC[16,17]. DIC budgets are constructed for February–November 1990, and February 1994 to February 1995 using the data in Fig. 2 and equations (3) and (4). Because CO_2 is a relatively soluble gas, the air–water exchange process by bubbles is relatively small and has been neglected[10]. The gas exchange mass transfer coefficient, G_{CO_2},

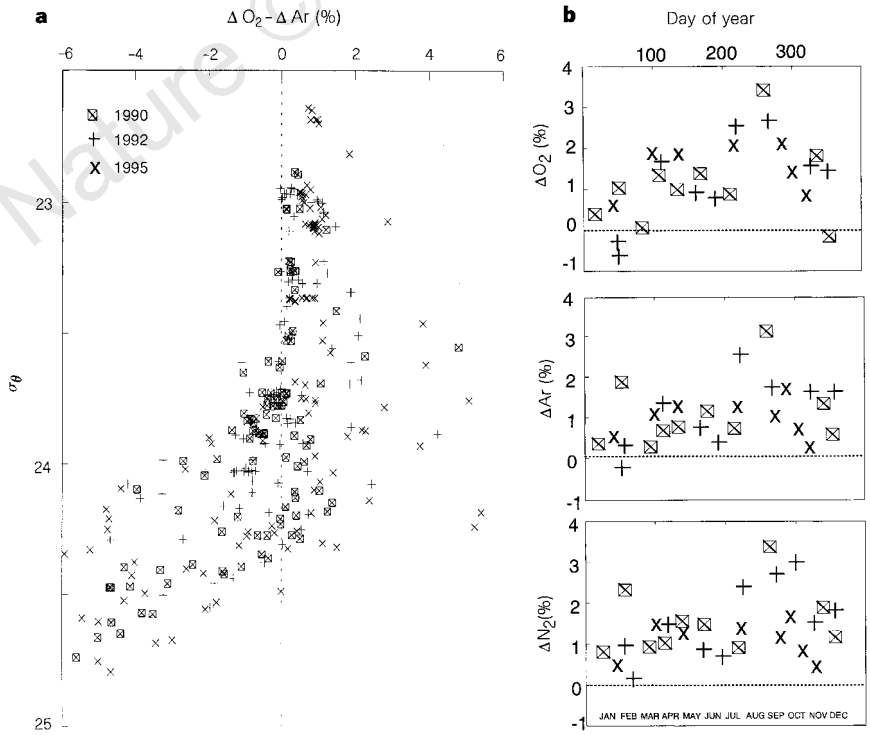


Figure 1 Oxygen, argon and nitrogen data in the upper water column at station ALOHA. Symbols represent different years: 1990 (⊠), 1992 (+), 1995 (×). **a**, The difference in the degree of saturation, Δ (in %), between oxygen and argon as a function of potential density, σ_θ, indicating a maximum in net biological oxygen production beneath the mixed layer (100 m is about $\sigma_\theta = 24$). **b**, The degree of saturation in the mixed layer as a function of time during the three sampling periods. Each point represents the mean of 3–10 measurements. We note that the waters are supersaturated during the entire year in spite of the diurnal temperature change of 4 °C at this latitude. Oxygen was determined by Winkler titration and other gases by ratios to oxygen measured by mass spectrometry (see ref. 28). For the relatively insoluble gases O_2, N_2 and Ar, the bubble term (B in equation (4)) is important in determining the gas supersaturation. As the mechanism of bubble process cannot be evaluated with only two inert-gas tracers, and there is evidence that in the subtropics simple air injection (where B is proportional to the partial pressure in the atmosphere, p_C) is not adequate[11,15], we assume that the mean value for the bubble term is determined by an equal combination of air injection and exchange across the surface of larger bubbles[9,11] (where B is proportional to the molecular diffusion coefficient (D), solubility (S) and mole fraction p_C, $D^{0.7}S^{0.35}p_C$). The error estimate of ±25% given in Table 1 spans the range between these two extremes.

Nature © Macmillan Publishers Ltd 1997

Nature © Macmillan Publishers Ltd 1997

and the horizontal velocity, V, were estimated as for O_2, Ar and N_2. With these values determined independently, we solved two equations for DIC and $DI^{13}C$ to determine the flux between the mixed layer and thermocline, F_h, and the net biological carbon production, J_{OC}. Details of this approach are described in ref. 16.

Measured annual rates of change of DIC and $DI^{13}C$ concentrations were of the same magnitude as their measurement errors of $\pm 2\ \mu mol\ kg^{-1}$ and $\pm 0.2‰$, respectively. Combination of the mass transfer coefficient and the observed degree of CO_2 gas undersaturation (Fig. 2b) resulted in a net CO_2 invasion rate of $0.6\ mol\ C\ m^{-2}\ yr^{-2}$. A meridional surface DIC flux of $-0.3\ mol\ C\ m^{-2}\ yr^{-1}$ was calculated from the horizontal velocity, V, and measured surface DIC gradients that increase to the north at a rate of $1\ \mu mol\ kg^{-1}$ per degree of latitude (P.Q., unpublished data). Rates of organic carbon production and flux from the thermocline necessary to balance the DIC fluxes and accommodate the stable-isotope data (Fig. 2) were 1.8 ± 0.9 and $1.5 \pm 1.0\ mol\ C\ m^{-2}\ yr^{-1}$, respectively. The origin of the error estimates is described in Table 1. Both the DIC and oxygen mass-balances indicate that net biological carbon and oxygen production at this location of the ocean are balanced by roughly equal fluxes between the atmosphere–water and mixed layer–thermocline interfaces.

The organic carbon mass balance consists of both particulate (POC) and dissolved (DOC) components. The rate of change of POC concentration is equal to the net formation rate of POC, J_{POC}, minus the fluxes out of the euphotic zone via gravitational settling, F_{POC}, and the net removal of POC by daily zooplankton migrations, F_{ZOO} (in $mol\ m^{-2}\ yr^{-1}$):

$$h(dPOC/dt) = J_{POC} - F_{POC} - F_{ZOO} \quad (5)$$

Particulate carbon fluxes measured by floating sediment traps[3] at 150 m (Fig. 3) vary between 0.4 and $0.9\ m\ C\ m^2\ yr^{-1}$ for the years in which other measurements were made. To compare these values with export fluxes determined by O_2 and DIC mass balances, we converted particulate carbon fluxes to organic carbon fluxes and extrapolated to 100 m, as described in Table 1.

Zooplankton respiration at depth represents an organic-carbon transfer out of the upper ocean for species that feed in the euphotic

Table 1 Net annual production of organic matter in the upper 100 m of the ocean at station ALOHA

			Organic carbon			
Year	O_2, N_2, Ar	DIC/$DI^{13}C$	POC	DOC	ZOO	ΣOC
1990	1.7 ± 1.4	1.5 ± 0.8	1.3 ± 0.4	0.8 ± 0.9		2.3 ± 1.0
1992	3.1 ± 2.2		0.8 ± 0.2	1.3 ± 1.2		2.3 ± 1.2
1994		1.8 ± 1.1			0.2 ± 0.1	
1995	3.1 ± 1.2		0.8 ± 0.1	0.5 ± 0.4	0.2 ± 0.1	1.5 ± 0.4
Mean	2.7 ± 1.7	1.6 ± 0.9				2.0 ± 0.9

Values (in $mol\ C\ m^{-2}\ yr^{-1}$) were determined by: mass balance of O_2, Ar and N_2 (column 2); mass balance of DIC and $DI^{13}C$ (column 3); and the sum (column 7) of fluxes of particulate organic carbon (POC; column 4), dissolved organic carbon (DOC; column 5), and zooplankton (ZOO; column 6) transport. Net oxygen production calculated from the model was transformed to carbon using a production quotient (PQ) of 1.25 which assumes that half of the net nitrogen uptake is as ammonia (PQ = 1.1) and half as nitrate (PQ = 1.4)[8,25]. For comparison with other fluxes, the POC flux at 150 m was multiplied by 0.9 to convert it to organic carbon flux[7] and extrapolated to 100 m using trap flux versus depth regressions established from similar sediment-trap studies in the subtropical Pacific Ocean that included the 100-m depth horizon[23]. The extrapolation increases the POC flux by 35%. Uncertainty estimates presented as (±) were determined in the oxygen and DIC mass balances using a Monte Carlo method in which deviations of the most important input values into equation (3) are assumed to be distributed in a gaussian way about the mean, with standard deviations equal to the uncertainty estimates. Values are chosen randomly and independently from these distributions and the equation solved repeatedly to determine the error or the dependent variables[6,26]. For the O_2, Ar and N_2 mass balance, input uncertainties (standard deviations) were: ±30% for the gas exchange parameter, G (this represents the difference between values generated using different correlations with wind speed[12,13] at $7\ m\ s^{-1}$, the mean value at station ALOHA); ±0.2% for the concentration of each of the gases and its degree of saturation[6]; and ±25% in the value of the bubble flux (this spans the range of values estimated by the two different mechanisms explained in Fig. 1 legend). For the DIC and $DI^{13}C$ mass balance, errors in the input values are the same for the gas exchange mass transfer coefficient, G, (±30%); and ±25% for the p_{CO_2} difference between the air and water. DIC and the $\delta^{13}C$ of DIC measurements have errors of $\pm 2\ \mu mol\ kg^{-1}$ and ±0.02‰, respectively. Organic carbon is assumed to have a $\delta^{13}C$ mean value and standard deviation of $-21 \pm 2‰$ (ref. 27). The error estimates for organic carbon fluxes represent: (1) for POC, the standard deviation of the monthly mean flux measurements (n = 9–11 for each year); (2) for DOC, combination of the error estimates of the oxygen flux, F_h, determined from the O_2, N_2 and Ar mass balances, and the standard deviation of the linear relationship between the DOC and O_2 in the 75–150 m interval ($\Delta DOC/\Delta O_2 = 0.58 \pm 0.37$); and (3) for ZOO, the error estimate of ±50% is from the standard deviation of the migratory of zooplankton biomass during monthly cruises in a given year. Mean values are unweighted averages of both the annual fluxes and their standard deviations. A random gaussian-weighted selection of values determined from the oxygen (2.7 ± 1.7) and DIC (1.6 ± 0.9) fluxes indicates that these distributions are indistinguishable ~50% of the time.

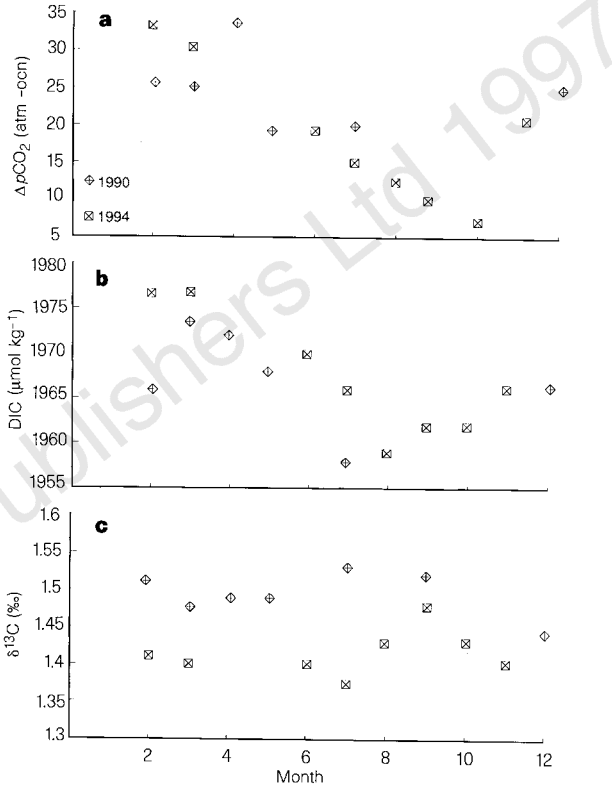


Figure 2 Measurements of dissolved inorganic carbon (DIC) species in the mixed layer at station ALOHA during 1990 (⊕) and 1994 (⊠). **a**, Δp_{CO_2} (p.p.m.) (defined as p_{CO_2}(atm) − p_{CO_2}(surface ocean)); here surface ocean p_{CO_2} values are calculated in 1990[3] and measured in 1994 (T. Takahashi, personal communication). **b**, DIC normalized to 35‰ salinity. **c**, $\delta^{13}C$ of DIC (‰ versus PDB). Details of the analytical methods used are given in refs 4 and 16. The procedure for writing the mass balances, including all important isotope ratios and pertinent isotope fractionation factors, are given in ref. 16.

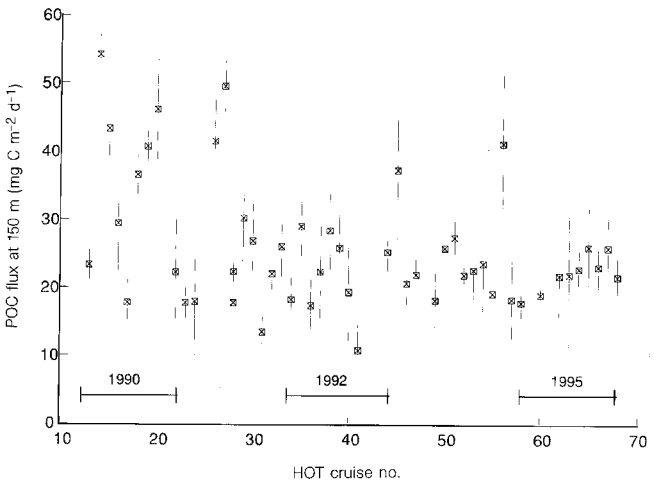


Figure 3 The particulate carbon flux at the depth of 150 m as a function of the Hawaii Ocean Time series (HOT) cruise number, with the 1990, 1992 and 1995 intervals indicated. Vertical error bars indicate the standard deviation of fluxes determined in 2–4 separate sediment-trap collector tubes at the 150-m reference depth deployed for 2–3 days on a free-drifting trap array. Methods are described in ref. 3.

Nature © Macmillan Publishers Ltd 1997

Nature © Macmillan Publishers Ltd 1997

zone at night and migrate to deeper waters during the day[18]. Based on measured day–night differences of zooplankton biomass, the size structure of the migrating zooplankton community (M.L., unpublished results), and empirical relationships for zooplankton metabolic rates as a function of animal size and environment temperature[19], we estimate the migrating zooplankton flux to be $0.2 \pm 0.1\,\mathrm{mol\,C\,m^{-2}\,yr^{-1}}$.

The strong vertical gradient in DOC in the upper 200 m of the subtropical ocean[20,21] suggests net production in the euphotic zone and net consumption in the upper thermocline. We estimate the importance of the flux of DOC to the organic carbon balance by comparing the vertical gradients of DOC and oxygen and multiplying the $\Delta DOC/\Delta O_2$ ratio by the flux of oxygen across the 100-m depth horizon, F_h. This portion of the organic-matter flux is, thus, dependent on results of the oxygen mass balance. The $\Delta DOC/\Delta O_2$ ratio across the 100-m horizon (~75–125 m) for nine different profiles in the years 1993–95 averaged 0.58 ± 0.37 (L.T., unpublished results) providing the driving force for ~40% of the total carbon flux out of the euphotic zone (Table 1).

Three organic-matter fluxes for the years 1990, 1992 and 1995 result in a mean of $2.0 \pm 0.9\,\mathrm{mol\,C\,m^{-2}\,yr^{-1}}$. This value is similar to that determined using the DIC and DI^{13}C mass balance (1.6 ± 0.9) and somewhat smaller than the estimate from oxygen mass balance (2.7 ± 1.7). The two most disparate of these three fluxes, however, are not significantly different (Table 1). We suggest that the present attainable accuracy of the biological pump at this location is roughly ±50%, and is limited primarily by uncertainty estimates of the individual fluxes. This may not be true for all ocean areas, however, as a recent comparison between organic carbon export determined by oxygen mass balance and POC + DOC fluxes at the Bermuda time-series station yielded a factor of two difference, with the latter being smaller[20].

We assume that our estimate of the organic-carbon export at station ALOHA ($\sim 2\,\mathrm{mol\,C\,m^{-2}\,yr^{-1}}$) is typical of the subtropical oceans, as it is probably more representative than the station at Bermuda with its very deep winter mixed layers. As the area of the subtropical oceans is ~60% of the total ocean area[22], the annual biological pump from this ocean province is $5–6\,\mathrm{Gt\,C\,yr^{-1}}$. Current estimates of the global ocean organic carbon pump based on sediment trap fluxes are $\sim 5\,\mathrm{Gt\,C\,yr^{-1}}$ ($1.2\,\mathrm{mol\,C\,m^{-2}\,yr^{-1}}$)[3,22,23]. Our value of $5–6\,\mathrm{Gt\,C\,yr^{-1}}$ for the subtropics alone indicates that these global estimates are almost certainly too low, as upwelling and coastal regions are believed to account for a significant organic-carbon export[22]. If we assume that recent model-derived estimates of the global ocean organic carbon pump ($10–11\,\mathrm{Gt\,yr^{-1}}$)[1,24] are correct, then the subtropical oceans may account for up to half of the global value. An urgent task for marine scientists is to understand the mechanisms that limit this organic-carbon export so that predictions of the response to changes in forcing can be made. □

Received 1 July; accepted 9 September 1997.

1. Sarmiento, J. L. & Siegenthaler, U. in *Primary Productivity and Biogeochemical Cycles in the Sea* (eds Falkowski, P. G. & Woodhead, A. D.) 317–332 (Plenum, New York, 1992).
2. Karl, D. M. & Lukas, R. The Hawaii Ocean Time-series (HOT) program: Background, rationale and field implementation. *Deep-Sea Res. II* **43,** 129–147 (1996).
3. Karl, D. M. *et al.* Seasonal and interannual variability in primary production and particle flux at Station ALOHA. *Deep-Sea Res. II* **43,** 539–569 (1996).
4. Winn, C. D., Mackenzie, F. T., Carrillo, C. J., Sabine, C. L. & Karl, D. M. Air–sea carbon dioxide exchange in the North Pacific subtropical gyre: Implications for the global carbon budget. *Glob. Biogoechem. Cycles* **8,** 157–163 (1994).
5. Quay, P. D. & Andersen, H. Organic carbon export rates in the Subtropical N. Pacific. *Eos* **76,** OS85 (1996).
6. Emerson, S., Quay, P. D., Stump, C., Wilber, D. & Schudlich, R. Chemical tracers of productivity and respiration in the subtropical Pacific Ocean. *J. Geophys. Res.* **100,** 15873–15887 (1995).
7. Sabine, C. L., Mackenzie, F. T., Winn, C. & Karl, D. M. The influence of air–sea exchange on the isotopic composition of oceanic carbon: Observations and modelling. *Glob. Biogeochem. Cycles* **9,** 637–652 (1995).
8. Laws, E. A. Photosynthetic quotients, new production and net community production in the open ocean. *Deep-Sea Res.* **38,** 143–167 (1991).
9. Keeling, R. On the role of large bubbles in air–sea exchange and supersaturation in the ocean. *J. Mar. Res.* **51,** 237–271 (1993).
10. Woolf, D. Bubbles and air–sea transfer velocity of gases. *Atmos. Ocean* **31,** 517–540 (1993).
11. Schudlich, R. & Emerson, S. Gas saturation in the surface ocean: The roles of heat flux, gas exchange and bubbles. *Deep-Sea Res. II* **43,** 569–591 (1996).
12. Liss, P. S. & Merlivat, L. in *The Role of Air–Sea Exchange in Geochemical Cycling* (ed. Buat-Ménard, P.) 112–127 (Reidel, Norwell, MA, 1986).
13. Wanninkhof, R. Relationship between wind speed and gas exchange over the ocean. *J. Geophys. Res.* **97,** 7373–7382 (1992).
14. Roden, G. I. On the subtropical frontal zone north of Hawaii in winter. *J. Phys. Oceanogr.* **10,** 342–362 (1980).
15. Jenkins, W. Using anthropogenic tritium and ^{3}He to study subtropical gyre ventilation and circulation. *Phil. Trans. R. Soc. Lond. A* **325** 43–61 (1988).
16. Zhang, J. & Quay, P. D. The total organic carbon export rate based on ^{13}C and ^{12}C of DIC budgets in the Equatorial Pacific region. *Deep-Sea Res. II* (in the press).
17. Broecker, W. S. & Peng, T. H. Gas exchange rates between air and sea. *Tellus* **XXVI,** 21–35 (1974).
18. Longhurst, A. R. & Harrison, W. G. The biological pump: profiles of plankton and consumption in the upper ocean. *Prog. Oceanogr.* **22,** 46–123 (1989).
19. Ikeda, T. Metabolic rates of epipelagic marine zooplankton as a function of body mass and temperature. *Mar. Biol.* **85,** 1–11 (1985).
20. Carlson, C. A., Ducklow, H. W. & Michaels, A. F. Annual flux of dissolved organic carbon from the euphotic zone of the northwest Sargasso Sea. *Nature* **371,** 405–408 (1994).
21. Tupas, L. M., Popp, B. N. & Karl, D. Dissolved organic carbon in oligotrophic waters: Experiments on sample preservation, storage and analysis. *Mar. Chem.* **41,** 207–216 (1993).
22. Eppley, R. W. & Peterson, B. J. Particulate organic flux and planktonic new production in the deep ocean. *Nature* **282,** 677–680 (1979).
23. Martin, J. H., Knauer, G. A., Karl, D. M. & Broenkow, B. B. VERTEX: Carbon cycling in the northeast Pacific. *Deep-Sea Res.* **34,** 267–285 (1987).
24. Six, K. D. & Maier-Reimer, E. Effect of plankton dynamics on the seasonal carbon fluxes in a ocean general circulation model. *Glob. Biogeochem. Cycles* **10,** 559–583 (1996).
25. Karl, D. M. *et al.* The role of dinitrogen fixation in the nitrogen budget of the subtropical North Pacific Ocean. *Nature* **388,** 533–538 (1997).
26. Quay, P. D., Emerson, S., Wilber, D. O. & Stump, C. The δ^{18}O of dissolved O_2 in the surface waters of the subarctic Pacific; a tracer of biological productivity. *J. Geophys. Res.* **98,** 8447–8458 (1993).
27. Goericke, R. & Fry, B. variations of marine plankton δ^{13}C with latitude, temperature and dissolved CO_2 in the world ocean. *Glob. Biogeochem. Cycles* **8,** 85–90 (1994).
28. Emerson, S., Quay, P. D., Stump, C., Wilber, D. & Knox, M. O_2, Ar, N_2 and ^{222}Rn in surface waters of the subarctic Pacific Ocean. *Glob. Biogeochem. Cycles* **5,** 49–69 (1991).

Acknowledgements. We thank C. Stump, D. Wilber and D. Hebel for technical work which helped make this study possible. This work was supported by the NSF.

Correspondence and requests for materials should be addressed to S.E. (e-mail: emerson@u.washington.edu).

Ice–volcano interaction of the 1996 Gjálp subglacial eruption, Vatnajökull, Iceland

Magnús T. Gudmundsson*, Freysteinn Sigmundsson† & Helgi Björnsson*

** Science Institute, University of Iceland, Dunhaga 3, 107 Reykjavik, Iceland*
† Nordic Volcanological Institute, University of Iceland, Grensasvegur 50, 108 Reykjavik, Iceland

Volcanic eruptions under glaciers can cause dangerous floods and lahars[1–3] and create hyaloclastite (fragmented glassy rock) mountains[4–8]. But processes such as the rate of heat transfer between ice and magma, edifice formation, and the response of the surrounding glacier are poorly understood, because of the lack of data. Here we present observations from the fissure eruption at Vatnajökull ice cap, Iceland, in October 1996. In the 13 days of the eruption 3 km^3 of ice were melted and the erupted magma fragmented into glass forming a hyaloclastite ridge 6–7 km long and 200–300 m high under 500–750 m of ice. Meltwater of temperatures of 15–20 °C flowed along a narrow channel at the glacier bed into the Grímsvötn subglacial lake for five weeks, before draining in a sudden flood, or jökulhlaup. Subsidence and crevassing of the ice cap occurred over the eruptive fissure and the meltwater path, whereas elsewhere the glacier surface remained intact, suggesting that subglacial eruptions do not trigger widespread basal sliding in warm-based glaciers.

Despite the lack of direct observations of subglacial eruptions, qualitative models of the formation of hyaloclastite mountains within glaciers were presented in the 1940s and 1950s[5–7] and have been advanced by more recent work[8–10]. These models are based on geological mapping and involve melting of the overlying ice and the emergence of a mountain within a water-filled depression confined by the surrounding glacier. The lowermost parts of the mountains are often made of pillow lavas, whereas the upper parts are

Nature © Macmillan Publishers Ltd 1997